

Active site structure of the catalase-peroxidases from *Mycobacterium tuberculosis* and *Escherichia coli* by extended X-ray absorption fine structure analysis

Linda Powers^{a,*}, Alex Hillar^b, Peter C. Loewen^b

^a National Center for the Design of Molecular Function, Utah State University, Logan, UT 84322-4155, USA

^b Department of Microbiology, University of Manitoba, Winnipeg, MB R3T 2N2, Canada

Received 24 January 2000; received in revised form 5 September 2000; accepted 7 September 2000

Abstract

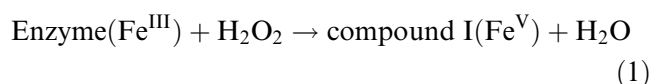
The catalase-peroxidase encoded by *katG* of *Mycobacterium tuberculosis* is a more effective activator of the antibiotic isoniazid than is the equivalent enzyme from *Escherichia coli*. The environment of the heme iron was investigated using X-ray absorption spectroscopy to determine if differences in this region were associated with the differences in reactivity. The variation in the distal side Fe–ligand distances between the two enzymes was the same within experimental error indicating that it was not the heme iron environment that produced the differences in reactivity. Analysis of variants of the *E. coli* catalase-peroxidase containing changes in active site residues Arg102 and His106 revealed small differences in Fe–water ligand distance including a shorter distance for the His106Tyr variant. The Arg102Leu variant was 5-coordinate, but His106Cys and Arg102Cys variants showed no changes within experimental error. These results are compared with those reported for other peroxidases. © 2001 Elsevier Science B.V. All rights reserved.

Keywords: Catalase-peroxidase active site; *Mycobacterium tuberculosis*; EXFAS

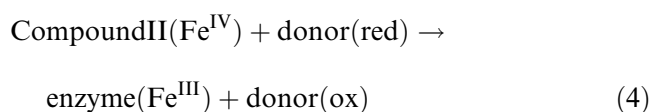
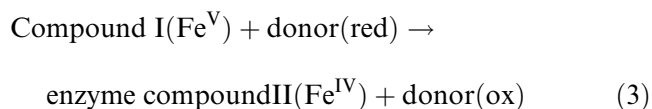
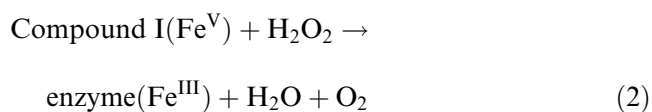
1. Introduction

Catalase-peroxidases are a class of hemoprotein enzymes involved in the oxidative defense repertoire of cells [1,2]. They function primarily as catalases to convert two molecules of hydrogen peroxide into water and oxygen via a two-step reaction cycle in which the substrate alternately acts to oxidize and then reduce the heme iron at the active site. As their

name suggests, they also exhibit a peroxidatic activity which begins with a similar reaction to the catalytic cycle involving hydrogen peroxide oxidizing the heme iron. The second step involves reduction of the heme iron by a hydrogen donor other than hydrogen peroxide. In detail, the sequence of reactions for generic catalases and peroxidases follow the schemes shown below in which reaction 1 is common to both and is followed by reaction 2 in the catalytic pathway or reactions 3 and 4 in the peroxidatic pathway:



* Corresponding author. Fax: +1-435-797-3328;
E-mail: lsp@biocat.ece.usu.edu



Oxidized donor species, as in horseradish peroxidase, may be free radicals. In catalases, the peroxidatic reactions 3 and 4 will occur only under conditions of low peroxide concentration in the presence of a suitable donor, because compound I is preferentially reduced via a one-step, two-electron reaction in which the substrate donor is usually a second molecule of hydrogen peroxide. At very high concentrations of hydrogen peroxide, both peroxidases and catalases can form an additional, reversibly inactivated species, known as compound II, at a formal oxidation state of Fe^{IV}. To date, the majority of catalase-peroxidases investigated have been bacterial in origin [2], although catalase-peroxidases from fungi have also been identified [3,4].

Recently, the role of the catalase-peroxidase of *Mycobacterium tuberculosis* (MtKatG) in the activation of the front-line antitubercular drug isoniazid (isonicotinic acid hydrazide, INH) has been the subject of intensive investigations. Considerable evidence indicates that MtKatG oxidizes INH to an electrophilic species which binds to, and inactivates, InhA, an acyl carrier protein reductase [5,6], or other potential targets [7] which cause inhibition of the synthesis of mycolic acids, which are long-chain fatty acids, required for the cell wall of *M. tuberculosis*.

Escherichia coli possesses a catalase-peroxidase (EcKatG, also known as HPI or hydroperoxidase I) with significant (~70%) homology to MtKatG. Purified EcKatG has been shown to have many physical and chemical similarities to MtKatG, including comparable kinetic parameters, subunit sizes, and susceptibility to classical heme enzyme inhibitors such as cyanide. Despite these similarities, EcKatG is not as proficient in the peroxidatic oxidation of INH [8], nor are *E. coli* cells susceptible to INH, even at

very high concentrations of the drug. On the other hand, MtKatG, when over-expressed in *E. coli*, results in the increased susceptibility of the cells to INH [9]. This suggests that the MtKatG is at least partially responsible for the cytotoxicity of the drug, even in a heterologous host, but also implies that there must be some structural differences between EcKatG and MtKatG proteins. It has recently been shown [10] that INH binds to MtKatG at a position about 12 Å from the active site heme iron. However, no catalase-peroxidase has been crystallized to date, making clear structural inferences about the mechanism of INH oxidation in EcKatG and MtKatG a matter of speculation based on the structures of plant peroxidases.

X-ray absorption spectroscopy (XAS) has been used to elucidate the nature of the heme active sites of a number of hemoproteins and has been instrumental in the development of theories of hemoprotein catalysis [11–25]. XAS provides information on the number and the average distance of ligands, their relative disorder, as well as information on allows inferences to be made about the interaction between the heme and the surrounding protein residues.

In an extensive X-ray absorption fine structure analysis (EXAFS) study of the peroxidases, catalases, and globins [11–25], the structure of the heme active site has been shown to differ between the peroxidases and the globins. The proximal histidine, which provides the only linkage between the heme and the protein backbone in most hemoproteins, is significantly closer to the iron (~0.15 Å) in the peroxidases and catalases than in the globins. A consequence of this is that the peroxidases and catalases have an increased charge density in the heme and an expanded average iron to heme nitrogen distance (Fe–N_p) to the globins. Substituent groups on the heme also alter the charge density of the heme active site and the distal pocket structure can exert steric constraints on the sixth axial ligand of the heme iron. These factors affect reactivity.

Differences in the structure of the heme active site are also observed between native forms of the various peroxidases [11,14,17–21,24,25]. The reactivity of hemoglobins towards oxygen binding has been described by high (R-state) or low (T-state) affinity forms. The iron to heme nitrogen average distance is expanded in the low affinity T-states compared to

the high affinity R-states. Peroxidase reactivity can similarly be described where a longer iron to heme nitrogen average distance correlates with increased peroxidase activity. Thus, differences in reactivity of hemeproteins can be at least partially attributable to differences in structure of the heme active site.

We have undertaken an EXAFS study to compare the heme active site structures of the MtKatG and the EcKatG enzymes and a number of EcKatG mutant variants to gain insight into whether the differences in reactivity can be attributable to differences in the heme active site structure.

2. Materials and methods

2.1. Materials

Common chemicals and biochemicals were from Sigma Chemical Co. or Fisher Scientific. Restriction nucleases, polynucleotide kinase, and T4 DNA ligase were from Gibco-BRL. The T7 dideoxy sequencing kit was obtained from Pharmacia.

2.2. Bacterial strains and plasmids

Construction of plasmid pAH1, used to express MtKatG, has been previously described [8]. The plasmid pBT22 [26] was used as the source for the *E. coli katG* gene. The 4.0 kb pBT22 *HindIII*–*HindIII* fragment, containing the *E. coli katG* gene, was excised and ligated into M13 phagemid pSK+ (Stratagene Cloning Systems), where the gene was under the control of the *lac* promoter. The resulting 7.0 kb vector was designated pAH6-1. Phagemids pSK+ and pKS– were used for subsequent subcloning, mutagenesis, sequencing, and recloning. *E. coli* strains NM522 (*supE thi Δ(lac-proAB) hsd-5 [F' proAB lacIq lacZΔ15]*) [27], JM109 (*recA1 supE44 endA1 hsdR17 gyrA96 relA1 thi Δ(lac-proAB)*) [28] and CJ236 (*dut-1 ung-1 thi-1 relA1/pCJ105 F'*) [29] were used as hosts for the plasmids and for generation of single-strand phage DNA using helper phage R408. *E. coli* strain UM262 *recA katG::Tn10 pro leu rpsL hsdM hsdR endI lacY* [30] was used for expression of the mutant *katG* constructs and isolation of the mutant EcKatG proteins.

2.3. Oligonucleotide-directed mutagenesis

Oligonucleotide primers were synthesized on a PCR-Mate synthesizer from Applied Biosystems. For His106 replacements, the sequence CAC at position 316 [31] was changed to CTG (Leu106) using 5'-TGGCCTGGCTGGGCGCGGGG and TGC (Cys106) using 5'-TGGCCTGGTGGCGCGGGG. For Arg102 replacements, the sequence CGT at position 304 was changed to CTG (Leu102) using 5'-TGTTTATTCTGATGGCCTGG and TGT (Cys102), using 5'-TGTTTATTTGTATGGCCTGG. A 147bp *EcoRI*–*ClaI katG* fragment, containing the codons for both His106 and Arg102, including nucleotides 194–341 of the *katG* sequence, was subcloned into pSK+ for mutagenization [29]. Sequences were confirmed [32] using double-stranded DNA and the protocols specified by the sequencing kit supplier. Mutagenized fragments were then recloned into pKS– containing *E. coli katG* (designated pAH8m), sequenced over the *EcoRI*–*ClaI* region to confirm the mutation, and then transformed into UM262 for expression.

2.4. Sample preparation

UM262 cells transformed with the appropriate plasmids were grown in 4–6-l batches of LB medium supplemented with 50 μM FeCl₃, and in the case of MtKatG preparation, 50 μM γ-aminolevulinic acid. Cells were grown overnight with good aeration at 37°C, or occasionally at 28°C in the case of mutant protein preparation. MtKatG was purified as previously described [8]. EcKatG and the mutant EcKatG proteins were purified as described [30], with the modification that DEAE-cellufine (Amicon) was used in place of DEAE–Sephadex A25. In cases where there was little catalase activity associated with the KatG protein, the purification was followed by sodium dodecyl sulfate–polyacrylamide gel electrophoresis. Samples were lyophilized for transport and, following rehydration, were packed in plexiglass holders and frozen for XAS measurements. Lyophilization and rehydration had no effect on the enzyme as determined by activity assays and polyacrylamide gel analyses before and after. Protein concentration was estimated to be less than 1 mM.

2.5. Optical absorption spectroscopy

Optical absorption spectra were obtained using either a Milton Roy MR3000 or a Pharmacia Ultrospec 4000 UV-Vis spectrophotometer, in 1 ml quartz semi-micro cuvettes. Samples were dissolved in 50 mM potassium phosphate, pH 7.0, unless otherwise stated.

2.6. Catalase assay and protein determination

Catalase activity was determined by the method of Rørth and Jensen [33] in a Gilson oxygraph equipped with a Clark electrode. One unit of catalase is defined as the amount that decomposes 1 μmol of H_2O_2 in 1 min in a 60 mM H_2O_2 solution (pH 7.0) at 37°C. Protein was estimated according to the methods outlined by Layne [34].

2.7. X-ray absorption measurements

X-ray absorption measurements were performed at the National Synchrotron Light Source on Beamline X-9 using Si(111) crystals which provide ~ 2 eV resolution at 7 keV. Protein samples and model compounds were maintained at $\sim -80^\circ\text{C}$ during X-ray exposure to minimize radiation damage [35]. A 13-element Ge detection system was used for fluorescence data collection. The spectra were averaged until the signal-to-noise ratio at ~ 7.9 keV ($k \sim 13 \text{ \AA}^{-1}$) was > 2 .

2.8. X-ray absorption data analysis

Data were analyzed according to previously described methods [12,16,36–40] which use the filtered first-shell data. These methods were chosen as considerable crystallography results on heme proteins and model compounds have shown that the largest differences/changes in bond distances occur in the first coordination shell. Furthermore, inclusion of the higher shells increases the errors in the fits, since higher shells have considerable lower signal-to-noise ratio than the first shell.

Briefly, the absorption below the edge was set equal to zero. The EXAFS modulations were isolated by background subtraction and normalization, k^3 multiplication which approximately equalizes the

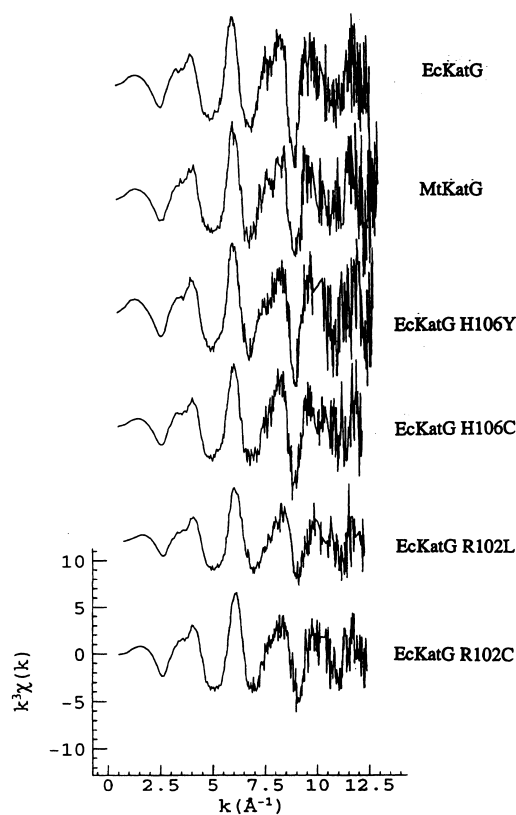


Fig. 1. EXAFS modulations (data after background subtraction and k^3 multiplication) for MtKatG, EcKatG, and EcKatG mutants. Note that the data has had instrumental glitches removed [12,16,36–40].

modulations in k -space (Fig. 1), and Fourier transformation which converts the data to distance space (Fig. 2). The contribution of each shell was isolated by application of a Fourier window filter and back-transformation. Thus, for each coordination shell, the amplitude contains the number of scattering atoms (N) and their Debye–Waller factors (σ^2) while the phase contains the average distance (r) and the threshold energy (E_0). Comparison of the sample amplitude and phase with those of carefully chosen model compounds having similar structure and for which the structure has been determined gives the sample parameters: r , N , $\Delta\sigma^2$, and ΔE_0 , where $\Delta = (\text{model} - \text{protein})$. The ‘goodness’ of the fit was judged by the sum of the residuals squared, ΣR^2 . It was not necessary to divide this quantity by the number of data points in the fit because the number of data points was the same for all fits.

In order to compare the results of the fitting pro-

Table 1
EXAFS analysis results

Protein	r (Å)	N^a	$\Delta\sigma^2$ (Å ²) ^b	ΔE_0^c (eV)	ΣR^2
<i>M. tuberculosis</i> KatG	2.03	5	2.5×10^{-3}	-0.8	2.0
	1.88	1	4.3×10^{-3}	-1.0	
	2.00	5	-2.2×10^{-3}	-0.6	2.1
	2.07	1	6.6×10^{-3}	-2.9	
	2.02^d	4	3.3×10^{-3}	-0.4	1.8
	1.88^e	1	4.9×10^{-3}	-1.6	
	2.10^f	1	3.4×10^{-3}	-2.5	
<i>E. coli</i> KatG	2.04	5	1.5×10^{-3}	-0.3	2.0
	1.94	1	3.9×10^{-3}	-1.8	
	2.00	5	1.5×10^{-3}	-0.7	1.8
	2.11	1	4.6×10^{-3}	0.8	
	2.02	4	5.6×10^{-3}	-0.1	1.0
	1.90	1	4.9×10^{-3}	-1.4	
<i>E. coli</i> KatG H106Y	2.15	1	8.3×10^{-3}	0	
	2.03	5	1.7×10^{-3}	0	4.3
	1.84	1	-6.2×10^{-3}	4.8	
<i>E. coli</i> KatG H106C	2.05	5	2.0×10^{-3}	-0.8	2.7
	1.90	1	6.9×10^{-3}	2.1	
	2.00	5	2.5×10^{-3}	0.2	2.0
	2.14	1	7.7×10^{-3}	-1.5	
	2.03	4	3.8×10^{-3}	-0.3	1.7
	1.90	1	-9.0×10^{-3}	3.9	
	2.16	1	8.5×10^{-3}	-1.0	
	2.00	5	1.4×10^{-3}	-0.2	2.9
	2.22 ^g	1	1.6×10^{-3}	8.8	
	2.04	4	1.6×10^{-3}	0.4	1.9
<i>E. coli</i> KatG R102L	1.92	1	6.6×10^{-3}	-1.6	
	2.20 ^g	1	-1.4×10^{-3}	6.4	
	2.02	4	1.5×10^{-3}	-1.8	3.1
	1.90	1	3.0×10^{-3}	8.0	
	2.04	5	2.1×10^{-3}	-1.0	2.2
<i>E. coli</i> KatG R102C	1.89	1	5.0×10^{-3}	4.5	
	1.99	5	4.0×10^{-3}	0.3	2.8
	2.10	1	6.5×10^{-3}	-2.9	
	2.00	4	4.0×10^{-3}	-0.2	1.8
	1.90	1	4.1×10^{-3}	5.8	
	2.11	1	6.7×10^{-3}	-2.5	

^a N values fixed.

^b $\Delta\sigma^2 = (\sigma_{\text{model}}^2 - \sigma_{\text{enzyme}}^2) \pm 35\%$.

^c $\Delta E_0 = (E_{0\text{model}} - E_{0\text{enzyme}}) \pm 2.0$ eV.

^d ± 0.015 Å.

^e ± 0.02 Å.

^f ± 0.03 Å.

^g Fe–S distance.

cedure, we must determine how much ΣR^2 values must differ for the fits to be considered statistically different. Following Powers and Kincaid [40], the number of degrees of freedom in the fit is related to the number of degrees of freedom in the data and the number of variable parameters in the fit.

Using a window width of 1.1 Å, three independent fitting variables per atom-type, and $\Delta k \sim 13$ Å⁻¹, ΣR^2 for two solutions having two atom-types must differ by a factor of at least 1.4 to be considered statistically different. The solution parameters must also be physically reasonable [12,16,36–40].

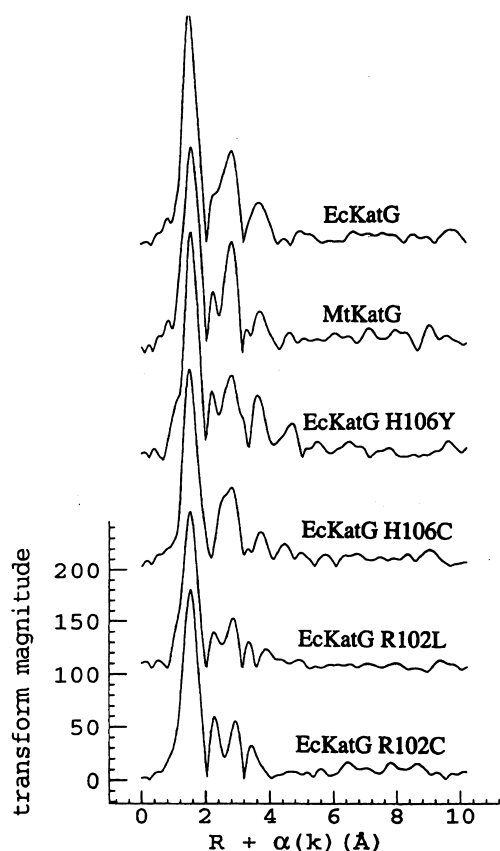


Fig. 2. Fourier transforms of the EXAFS data of Fig. 1 for MtKatG, EcKatG, and EcKatG mutants.

After possible solutions were found for each contribution to the first shell (Fe–N_p (pyrrole nitrogens), Fe–N_e (proximal nitrogen), and Fe–X (distal ligand)), a three atom-type consistency test was carried out using all three sets of scatterers with *r* and *N* held constant in order to verify that the three distances actually coexist in the data. Note that the number of variables in this consistency test is the same as that for the two atom-type fits described above. The sum of residuals squared for the three atom-type consistency test must be smaller than those obtained for the two atom-type solutions. To ensure that the three distances obtained from the above steps constitute a true minimum, each distance was allowed to vary individually in the three atom-type procedure. In each case, the residuals of the consistency test were comparable to the estimated error over the entire *k*-range.

Error estimation was obtained from the correlation and Hessian matrices of the nonlinear least

squares fits and by varying each parameter in the fit with the others held constant until the ΣR^2 doubled. The fitting results reported in Table 1 have used these methods and the best solutions as judged by these criteria are in bold type. Fig. 3 shows the comparison of the data and the best fit for EcKatG. The residuals are comparable to the noise in the data.

The Fe–N/O model compounds were Fe⁺³-bis-(imidazole-tetraphenylporphinato)chloride [41], and Fe⁺³-acetylacetonate [42]. The Fe–S model compound was Fe[CS₂:N-(CH₂)₄]₃ [43,44]. Data for these were collected under identical conditions and analyzed using the same procedures as those used for the enzyme samples.

In order to demonstrate that these methods are capable of resolving the reported distances in the

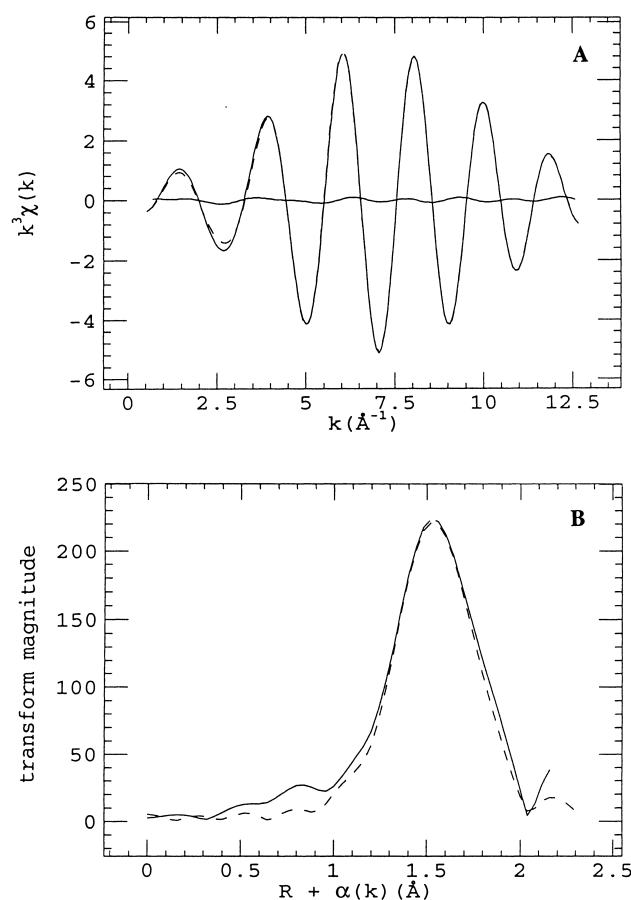


Fig. 3. Comparison of the first-shell filtered data of EcKatG (A) and its Fourier transform magnitude (B) with that obtained by the fit in bold type of Table 1. The residuals are also shown in panel A.

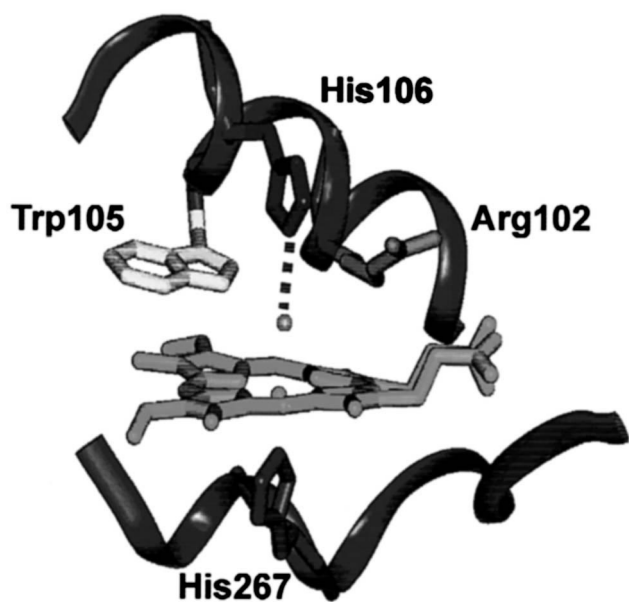


Fig. 4. Representation of the heme environment of the catalase-oxidase based on the structure of cytochrome *c* peroxidase showing Arg102, Trp105 and His106. The residue numbering is that of *E. coli* KatG. The distal or sixth ligand water molecule is shown coordinated between the heme iron and the imidazole ring of His106. The imidazole of His267 is the proximal side ligand of the heme.

data, data having the same parameters as those found for the experimental data were synthesized using the amplitudes and phases from a model compound. Gaussian noise was added in the amount contained in the experimental data and these synthetic data were then analyzed. Distances like those reported for the experimental data can clearly be reliably distinguished [36].

3. Results

3.1. Mutant catalase selection

The homology between EcKatG and other peroxidases [45] was used as the basis for selecting His106 and Arg102 (Fig. 4) of EcKatG (analogous to His52 and Arg48 of CCP) to be replaced with Leu and Cys residues. A water molecule, also hydrogen bonded to the imidazole of His52, is the distal side sixth ligand in CCP, and presumably in KatG as well, as shown in Fig. 4. This water is replaced by the substrate hydrogen peroxide resulting in initiation of a base-

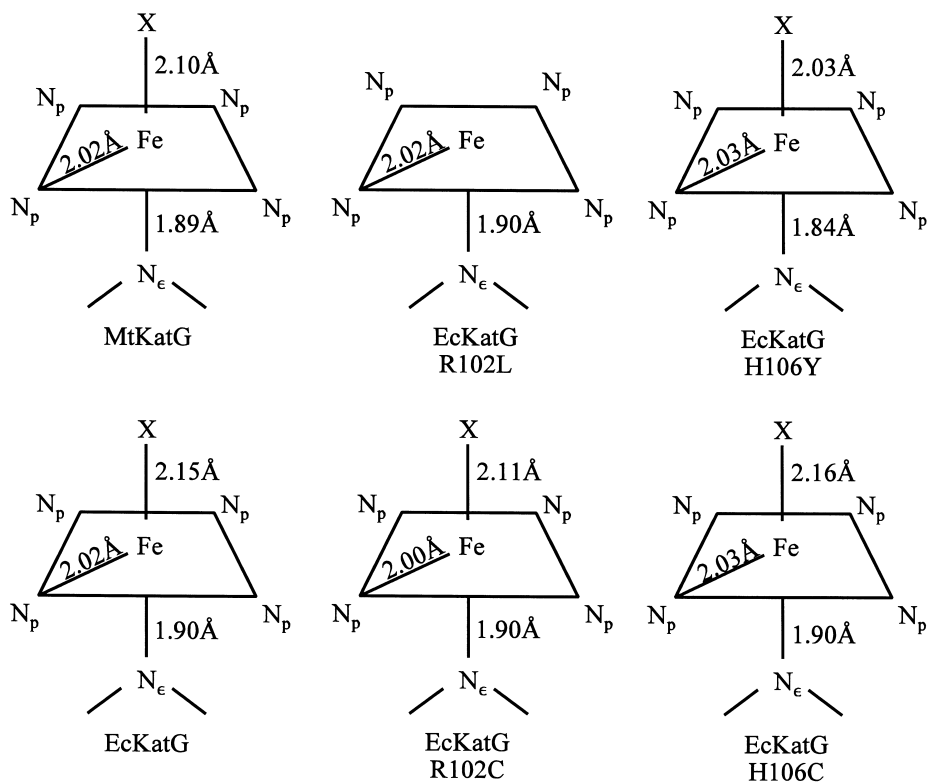


Fig. 5. Pictorial representation of the best solutions for MtKatG, EcKatG, and EcKatG variants.

catalyzed reaction by His106 leading to formation of compound I. Arg102 is thought to aid in the formation of compound I by stabilizing the transition state and promoting the heterolytic scission of the O–O bond of the peroxide coordinated between the heme iron and the distal His. A detailed characterization of these mutants is in preparation.

3.2. EXFAS results

The results of the EXFAS analysis are summarized in Table 1 and pictorially in Fig. 5.

The first coordination shells of MtKatG and EcKatG are very similar for the Fe–N_p average distance and the Fe–N_ε distance. Although the Fe–H₂O distances differ by 0.05 Å, this difference lies at the extreme of our conservative error estimate which includes both experimental and fitting errors. The local heme active site structure of both enzymes are similar to those of other peroxidases and catalases [11,13–25,39]. Note that the higher coordination shells in Fig. 2 are similar, but not identical, as are the optical absorption spectra of EcHPI and MtHPI [8].

The optical absorption spectrum (Fig. 6) of the R102L variant shows a distinctive shoulder to the Soret band in the 380 nm region as compared with the EcKatG wild type which is very similar to the case for the equivalent mutant in HRP-C* R38L that is 5-coordinate. The EXAFS data clearly show that the R102L mutant lacks a sixth ligand. Any attempt to fit this data with more ligands triples the ΣR^2 , even though the average Fe–N_p and Fe–N_ε distances are unchanged from those of EcKatG. When this Arg is replaced by Cys, the mutant R102C is six-coordinated, but the iron is in a low-spin state. The red shift of the Soret maximum in the absorbance spectrum, combined with a broadening of the bands in the visible region of the spectrum (Fig. 6), is reminiscent of the HRP-C* H42R mutant, which is also hexacoordinate and characterized via resonance Raman spectroscopy to have a low spin heme [46]. This sixth ligand can be either oxygen or nitrogen, as the EXAFS method cannot distinguish neighboring atoms in the periodic table. The higher shells are consistent with an additional His-ring contribution [47] as compared to the 5-coordinated R102L mutant and EcKatG (Fig. 2) making the imidazole of His106 a candidate for the sixth ligand. Water oxygen or a

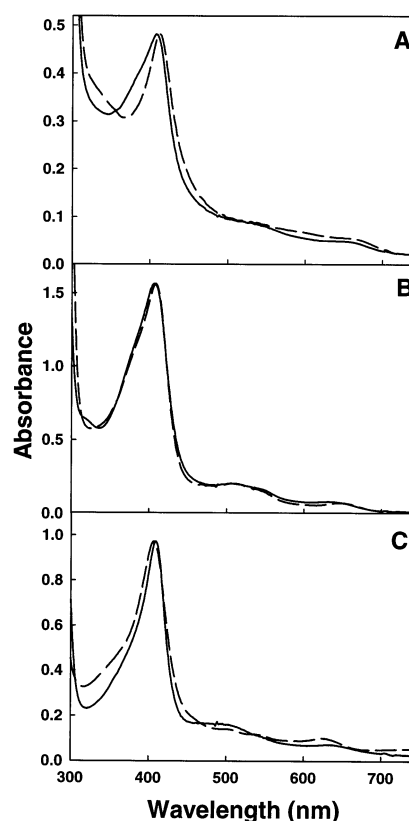


Fig. 6. Optical absorption spectra of EcKatG and its mutant variants. Spectra were obtained using 1–5 mg/ml solutions in 50 mM potassium phosphate buffer (pH 7.0) at room temperature. (A) Arg102Leu, solid line; Arg102Cys, dashed line. (B) His106Cys, solid line; His106Tyr, dashed line. (C) MtKatG, solid line; bovine liver catalase, dashed line. The spectrum of MtKatG differs slightly from the spectrum of EcKatG in being slightly blue-shifted in both the Soret (407 nm) and charge transfer (630 nm) regions (8).

smaller, less rigid, group, would cause little or no change in the outer shells. In any event, sulfur can be excluded in the sixth ligand position because it increases the ΣR^2 by about a factor of 2 and the ΔE_0 becomes large (9.5 eV), bordering on physical unreasonableness. The axial ligand distances are similar to those of EcKatG, but the average Fe–N_p distance is smaller as expected for a low-spin state of the iron.

The substituted Tyr in the H106Y variant likely participates in formation of the distal or sixth ligand of the iron as the higher shells are consistent with an additional Tyr-ring contribution. Both axial ligand distances are shortened as might be expected from the additional electron density provided by a Tyr–

oxygen ligand [17,19,47,48]. The Cys substitution for the distal His, H106C, does not change the first coordination shell distances within experimental error, but the higher shells are affected. If the distal ligand in H106C is assumed to be sulfur, the ΣR^2 is as good as that for oxygen or nitrogen ligation and all the fitting parameters are physically reasonable. However, 2.16 Å is too short for a Fe(heme)–S coordination distance, making a pure S coordination unlikely, although a mixture of both oxygen/nitrogen and sulfur ligation cannot be eliminated. The optical data (Fig. 6) for the His mutants shows that both are very similar to EcKatG, with slightly higher absorption in the 350–400 nm regions, but otherwise identical Soret maxima, further indicating that S is unlikely to be the distal or sixth ligand. The shifted positions of the charge transfer bands in the visible region of the spectra indicate some degree of disruption in the normal hydrogen bonding network in the vicinity of the heme, relative to EcKatG [49].

4. Discussion

Both *E. coli* and *M. tuberculosis* encounter H_2O_2 in their natural environments [50,51], and the primary role of KatG is to break down hydrogen peroxide, thereby preventing the formation of cytotoxic hydroxyl radicals. Despite this role, the enzyme is not essential for growth and the widespread use of INH to combat *M. tuberculosis* has resulted in the identification of an abundance of KatG-deficient mutants because the absence of the enzyme imparts resistance to INH [9,52]. The fact that EcKatG is not as effective as MtKatG at imparting INH sensitivity [9], a fact that was corroborated by the greater peroxidatic activity of MtKatG [8], suggested that the two proteins might differ with respect to their electron donor binding sites and that these differences may be reflected in a small, but possibly real, difference in the distal ligand distance. The high degree of similarity, if not identity (within experimental error), of the EcKatG and MtKatG heme iron environments shows conclusively that this region of the enzymes is not the source of the catalytic differences.

In view of the similarity between EcKatG and MtKatG in the heme iron environment, it is worthwhile to compare these results with those for other

peroxidases. The Fe–N_p average distance of MtKatG and EcKatG is similar to that of the other peroxidases (*Arthrobacter ramosus* peroxidase [11,14], microperoxidase MP8 [11,14], *Coprinus macrorhizus* peroxidase [11,14], and myeloperoxidase [25]). Sinclair et al. [17,18] have shown that the lignin peroxidase system, including both the lignin peroxidases and the Mn-dependent peroxidases, from *Phanerochaete chrysosporium* (Burd) and cytochrome *c* peroxidase have a longer Fe–N_p average distance than those of other peroxidases [11] and this may be responsible for the more electron-deficient heme observed in electrochemical studies [53]. In turn, this may be a contributing factor to the extremely high redox potential exhibited by the lignin peroxidase system. In particular, the first coordination shell of MtKatG is identical within experimental error to that of myeloperoxidase [25] and to catalase [12,48], even though catalase has tyrosine as a proximal ligand instead of histidine. Other peroxidases (e.g., lactoperoxidase, *C. macrorhizus* peroxidase, *A. ramosus* peroxidase, and cytochrome *c* peroxidase (MI)) also exhibit a similar Fe–H₂O distance. These results are in agreement with those of electron paramagnetic resonance spectroscopy [10]. This distance in EcKatG is more similar to the lignin peroxidase system.

The changes introduced on the proximal and distal side of the heme of EcKatG cause changes in the heme environment similar to those observed in variants of other peroxidases. The most dramatic effect was observed in the R102L variant in which the distal ligand is lost with no accompanying changes in the Fe–N_p or Fe–N_e ligand distances. Equivalent variants of both cytochrome *c* peroxidase (MI) [54] and HRP-C* R38L [46] are similarly 5-coordinate. The outer coordination shells and reduction of the Fe–X distance in the R102C variant are associated with a His coordinated low-spin heme iron similar to a 6-coordinate low-spin mutant of cytochrome *c* peroxidase (MI) which has the distal His coordinated to the iron at pH > 7.5 [54].

In addition to being similar (although not identical) to each other, the absorbance spectra of the EcKatG and MtKatG enzymes are similar to the spectra reported for other catalase-peroxidases [55,56], and they are consistent with the similarity in structures suggested by EXFAS data presented here (Fig. 5). Perhaps, not surprisingly, considering

the bifunctional nature of the enzymes, the spectra have features suggestive of both catalase and peroxidase spectra. For example, the Soret bands of EcKatG and MtKatG (408 nm) are red-shifted compared to HRP and HRP-C* (402 nm; [46]), with similarity to the Soret bands classically ascribed to blood and liver catalases (406 nm; [57]), while the main charge transfer band beyond 600 nm in the visible region of the spectrum for the MtKatG protein is found to be intermediate (628 nm) between the expected positions for the same bands of catalases (622 nm) and peroxidases (640 nm), including EcKatG (639 nm).

Even though the 0.05 Å longer Fe–H₂O distance of EcKatG compared to that of MtKatG is within our experimental error estimate, this difference is at the extreme and this estimate is conservative. It is worthwhile to consider the possibility that this difference may be real. If so, changes in the Fe–H₂O ligand distance should be reflected in the absorbance spectra. Two regions of the absorbance spectra correlate with changes in the Fe–H₂O ligand distance. In the first, the charge transfer band of the R102L variant, which lacks the sixth Fe–H₂O ligand, exhibits the greatest red shift to 650 nm. This is supported by the observation of a 0.05 Å longer Fe–H₂O ligand distance in EcKatG which is accompanied by a red shift to 639 nm. The second region is the shoulder on the Soret peak at 380 nm which decreases in prominence in the order R102L, EcKatG and MtKatG.

The spectral and EXAFS data point to only small differences in the heme iron environment between the EcKatG and the MtKatG enzymes, suggesting that subtle differences in the protein structures beyond the immediate redox center of the enzymes are responsible for the differences in how they interact with INH. This conclusion is consistent with the report that INH binds to MtKatG about 12 Å from the active site heme iron [10] and with NMR data showing that aromatic donor complexes in HRP-C are 8.4–12 Å from the heme iron [58]. The observation that EcKatG is much less proficient in producing INH derived free radicals compared to MtKatG in the presence of excess INH [8] may therefore be due to reduced affinity of the EcKatG donor binding site for INH compared to the binding site in MtKatG, rather than to any significant difference in active site heme structure. The apparent K_m values of 3.9 and 5.8 mM H₂O₂, respectively for EcKatG and MtKatG, used in

this work (data not shown and see [56,57,59–63]) also suggest little difference in the heme environment where the H₂O₂ binds. The differences in apparent k_{cat} values (1.6×10^4 s⁻¹ and 1.9×10^3 s⁻¹ for EcKatG and MtKatG, respectively) reflect the greater ease of the catalytic reaction and resultant specific activity of former enzyme. Peroxidatic reaction kinetic data is less readily available for comparison.

Acknowledgements

This work was supported by Grant OGP 9600 from the Natural Sciences and Engineering Research Council of Canada (to P.C.L.) and Utah State University (to L.P.).

References

- [1] K.G. Welinder, *Biochim. Biophys. Acta* 1080 (1991) 215–220.
- [2] P.C. Loewen, in: J.G. Scandalios (Ed.), *Oxidative Stress and the Molecular Biology of Antioxidant Defenses*, Cold Spring Harbor Laboratory Press, Cold Spring Harbor, NY, 1997, pp. 273–308.
- [3] M.W. Fraaije, H.P. Roubroeks, W.R. Hagen, W.J.H. Van Berkel, *Eur. J. Biochem.* 235 (1996) 192–198.
- [4] E. Levy, Z. Eyal, A. Hochman, *Arch. Biochem. Biophys.* 296 (1992) 321–327.
- [5] A. Banerjee, E. Dubnau, A. Quémard, V. Balusubramanian, K.S. Um, T. Wilson, D. Collins, G. de Lisle, W.R. Jacobs Jr., *Science* 263 (1994) 227–230.
- [6] D.A. Rozwarski, G.A. Grant, D.H.R. Barton, W.R. Jacobs Jr., J.C. Sacchettini, *Science* 279 (1998) 98–102.
- [7] K. Mdluli, D.R. Sherman, M.J. Hickey, B.N. Kreiswirth, S. Morris, C.K. Stover, C.E. Barry III, *J. Infect. Dis.* 174 (1996) 1085–1090.
- [8] A. Hillar, P.C. Loewen, *Arch. Biochem. Biophys.* 323 (1995) 438–446.
- [9] Y. Zhang, B. Heym, B. Allen, D. Young, S. Cole, *Nature* 358 (1992) 591–593.
- [10] N.L. Wengenack, S. Todorovic, L. Yu, F. Rusnak, *Biochemistry* 37 (1998) 15825–15834.
- [11] L. Powers, *Molecular Electronics and Molecular Electronic Devices 3*, CRC Press, Boca Raton, FL, 1994, p. 211.
- [12] B. Chance, L. Powers, Y. Ching, T.L. Poulos, G. Schonbaum, L. Yamazaki, K.G. Paul, *Arch. Biochem. Biophys.* 235 (1984) 596–611.
- [13] L. Powers, A. Naqui, C. Kumar, Y. Ching, B. Chance, *J. Biol. Chem.* 263 (1988) 7159–7163.
- [14] L. Powers, R. Sinclair, B. Chance, K. Reddy, I. Yamazaki, in: B. Chance, J. Deisenhofer, S. Ebashi, D. Goodhead, J.

- Helliwell, H. Huxley, T. Iizuka, J. Kirz, T. Mitsui, E. Rubenstein, N. Sakabe, T. Sasaki, G. Schmahl, H. Stuhmann, K. Wutrich, G. Zaccai (Eds.), *Synchrotron Radiation in the Biosciences*, Clarendon, New York, 1994, pp. 302–312.
- [15] M. Chance, L. Parkhurst, L. Powers, B. Chance, *J. Biol. Chem.* 261 (1986) 5689–5692.
- [16] M. Chance, L. Powers, T. Poulos, B. Chance, *Biochemistry* 25 (1986) 1259–1265.
- [17] R. Sinclair, L. Powers, J. Bumpus, A. Albo, B. Brock, *Biochemistry* 31 (1992) 4892–4900.
- [18] R. Sinclair, B. Copeland, Y. Yamazaki, L. Powers, *Biochemistry* 34 (1995) 13176–13182.
- [19] R. Sinclair, S. Hallam, M. Chen, B. Chance, L. Powers, *Biochemistry* 35 (1996) 15120–15128.
- [20] C.-S. Chang, I. Yamazaki, R. Sinclair, S. Khalid, L. Powers, *Biochemistry* 32 (1993) 923–928.
- [21] C.-S. Chang, R. Sinclair, S. Khalid, I. Yamazaki, S. Nakamura, L. Powers, *Biochemistry* 32 (1993) 2780–2786.
- [22] Z. Farhangrazi, R. Sinclair, I. Yamazaki, L. Powers, *Biochemistry* 34 (1995) 14970–14974.
- [23] Z. Farhangrazi, M. Fossett, L. Powers, W. Ellis, *Biochemistry* 34 (1995) 2866–2871.
- [24] B. He, R. Sinclair, R. Makino, G. Schonbaum, L. Powers, Y. Yamazaki, *Biochemistry* 35 (1996) 2413–2420.
- [25] K. Yue, K. Taylor, J. Kinkade, R. Sinclair, L. Powers, *Biochim. Biophys. Acta* 1338 (1997) 282–294.
- [26] B.L. Triggs-Raine, P.C. Loewen, *Gene* 52 (1987) 121–128.
- [27] D.A. Mead, E.S. Skorupa, B. Kemper, *Nucleic Acids Res.* 13 (1985) 1103–1118.
- [28] C. Yanisch-Perron, J. Vietra, J. Messing, *Gene* 33 (1985) 103–119.
- [29] T.A. Kunkel, J.D. Roberts, R.A. Zakour, *Methods Enzymol.* 154 (1987) 367–382.
- [30] P.C. Loewen, J. Switala, M. Smolenski, B.L. Triggs-Raine, *Biochem. Cell. Biol.* 68 (1990) 1037–1044.
- [31] B.L. Triggs-Raine, B.W. Doble, M.R. Mulvey, P.A. Sorby, P.C. Loewen, *J. Bacteriol.* 170 (1988) 4415–4419.
- [32] F.S. Sanger, S. Nicklen, A.R. Coulson, *Proc. Natl. Acad. Sci. USA* 74 (1977) 5463–5467.
- [33] M. Rørth, P.K. Jensen, *Biochim. Biophys. Acta* 139 (1967) 171–173.
- [34] E. Layne, *Methods Enzymol.* 3 (1957) 447–454.
- [35] B. Chance, P. Angiolillo, E. Yang, L. Powers, *FEBS Lett.* 112 (1980) 178–182.
- [36] P. Lee, P. Citrin, P. Eisenberg, B. Kincaid, *Rev. Mod. Phys.* 53 (1981) 769–806.
- [37] L. Powers, *Biochim. Biophys. Acta* 683 (1982) 1–38.
- [38] L. Powers, J. Sessler, G. Woolery, B. Chance, *Biochemistry* 23 (1984) 239–244.
- [39] B. Chance, R. Fischetti, L. Powers, *Biochemistry* 22 (1983) 3820–3829.
- [40] L. Powers, B. Kincaid, *Biochemistry* 28 (1989) 4461–4468.
- [41] D. Collins, R. Countryman, J. Hoard, *J. Am. Chem. Soc.* 94 (1972) 2066–2072.
- [42] J. Iball, C. Morgan, *Acta Cryst. B* 23 (1976) 239–244.
- [43] P. Healy, A. White, *J. Chem. Soc. (Lond.) Dalton Trans.* (1972) 1163–1171.
- [44] B. Teo, R. Shulman, G. Brown, A. Meixner, *J. Am. Chem. Soc.* 101 (1979) 5624–5631.
- [45] K.G. Welinder, *Curr. Opin. Struct. Biol.* 2 (1992) 388–393.
- [46] B.D. Howes, J.N. Rodriguez-Lopez, A.T. Smith, G. Smulevich, *Biochemistry* 36 (1997) 1532–1543.
- [47] H.L. Tang, B. Chance, A. Mauk, L. Powers, K. Reddy, M. Smith, *Biochim. Biophys. Acta* 1206 (1994) 90–96.
- [48] M. Chen, R. Sinclair, S. Hallam, L. Powers (2001) in preparation.
- [49] G. Smulevich, F. Neri, M.P. Marzocchi, K.G. Welinder, *Biochemistry* 35 (1996) 10576–10585.
- [50] M. Ma, J.W. Eaton, *Proc. Natl. Acad. Sci. USA* 89 (1992) 7924–7928.
- [51] B.M. Babior, in: *Oxygen and Life*, R. Soc. Chem. Special Publication no. 39, Whitstable Litho, Whitstable, UK, 1981.
- [52] J.M. Musser, V. Kapur, D.L. Williams, B.N. Kreiswirth, D. van Soolingen, J.D.A. van Embden, *J. Infect. Dis.* 173 (1996) 196–202.
- [53] C.D. Millis, D. Cai, M.T. Stankovich, M. Tien, *Biochemistry* 28 (1989) 8484–8489.
- [54] L. Vitello, J. Erman, M. Miller, J. Wang, J. Kraut, *Biochemistry* 32 (1993) 9807–9818.
- [55] M. Mutsuda, T. Ishikawa, T. Takeda, S. Shigeoka, *Biochem. J.* 316 (1996) 251–257.
- [56] F. Cendrin, H.M. Jouve, J. Gaillard, P. Thibault, G. Zaccai, *Biochim. Biophys. Acta* 1209 (1994) 1–9.
- [57] P. Nicholls, G.R. Schonbaum, in: P.D. Boyer, H. Lardy, K. Myrback (Eds.), *The Enzymes*, vol. 8, 2nd ed., Academic Press, London, 1963, pp. 147–222.
- [58] N.C. Veitch, *Biochem. Soc. Trans.* 23 (1995) 232–240.
- [59] A. Claiborne, I. Fridovich, *J. Biol. Chem.* 254 (1979) 4245–4252.
- [60] J.A. Marcinkeviciene, R.S. Magliozzo, J.S. Blanchard, *J. Biol. Chem.* 270 (1995) 22290–22295.
- [61] J.M. Nagy, A.E.G. Cass, K.A. Brown, *J. Biol. Chem.* 272 (1997) 31265–31271.
- [62] K. Johnsson, W.A. Froland, P.G. Schultz, *J. Biol. Chem.* 272 (1997) 2834–2840.
- [63] B. Saint-Joanis, H. Souchon, M. Wilming, K. Johnsson, P.M. Alzari, S.T. Cole, *Biochem. J.* 338 (1999) 753–760.